applied sciences

MDPI

Communication

Performance Simulation and Compression Cost Estimation of CO_2 Membrane Capture at Low Feed Concentrations

Thomas Ruh * and Christoph Rameshan

Chair of Physical Chemistry, Montanuniversität Leoben, 8700 Leoben, Austria
* Correspondence: thomas.ruh@unileoben.ac.at

Featured Application

This work aims to provide cost estimates for membrane capture of CO_2 from low-concentration flue gas based on electricity cost of feed stream compression.

Abstract

Carbon capture and utilization (CCU) is a promising approach to mitigating the effects of rising CO_2 levels due to industrial use of fossil fuels—particularly for industries that cannot reduce process-related emissions to zero. Although common CO_2 capture technologies based on absorption or adsorption have been well established and extensively researched, these methods require substantial investments in plant upgrades. Membrane capture is a possible alternative. While comparative studies have investigated membrane-capture efficiency at medium or high CO_2 concentrations—e.g., in retrofitting coal power plants—assessments of membrane performance at low CO_2 concentrations are rare. In this study, the performance of CO_2 capture membranes specifically for low-concentration flue gas is modeled, and the effects of membrane area, thickness, and pressure ratio are investigated. In addition, the electricity cost of compressing feed streams is used as an estimator of CO_2 capture cost per ton of CO_2 captured, thereby assessing the viability of membrane capture as retrofit option for small- and mid-sized companies seeking to reduce CO_2 emissions. For the membrane configurations and feed-gas CO_2 concentrations investigated (1–5%), estimated CO_2 capture costs range from 100 to 1200 € per ton of CO_2 captured. This wide range highlights the need for more sophisticated retrofit approaches.

Keywords: carbon capture; membranes; modeling; compression cost estimation

Check for updates

Academic Editor: Nikolaos Koukouzas

Received: 10 September 2026
Revised: 21 October 2026
Accepted: 25 October 2026
Published: 29 October 2026

Copyright: © 2026 by the authors. Licensee MDPI, Basel, Switzerland. This article is an open access article distributed under the terms and conditions of the Creative Commons Attribution (CC BY) license.

1. Introduction

Ever since the industrial revolution, the utilization of fossil fuels as an energy source has continuously increased, leading to atmospheric carbon dioxide (CO_2) concentration above 400 ppm [1]. The obvious consequences of these rising CO_2 levels—higher average temperatures and extreme weather events including droughts, heat waves, and storms—are compounded by phenomena such as refugee movements, loss of biodiversity, erosion and desertification ... [2]. To combat these effects, global programs and initiatives like the "European Green Deal" [3] are necessary to mitigate long-term damage and find solutions for the problems caused by CO_2 in our atmosphere.

Carbon capture and utilization (CCU) is a promising way to address CO_2 emissions. By using atmospheric CO_2 as a carbon feedstock to produce base chemicals like methanol [4] or syngas (a mixture of carbon monoxide and hydrogen) [5], the CO_2 levels either genuinely go down, as CO_2 is taken from the atmosphere, converted, and stored, or at least do not rise

further if those chemicals are used, as no "new" CO_2 is released (this depends on the use of the chemicals further down the line) [6]. This approach is especially useful for industries where emissions cannot be reduced to zero due to process-inherent CO_2 emissions, such as concrete production [7] and biomass gasification [8].

Carbon capture from flue gas is the initial step in all CCU processes—CO_2 needs to be separated from flue gas streams and potential impurities need to be removed. Processes based on absorption (using liquid sorption agents, e.g., amines or alkaline solutions) or adsorption (using solid agents, e.g., zeolites, resins, or metal–organic frameworks) to extract CO_2 from flue gas are well established both for scrubbing and gas separation. However, one of the major drawbacks of these technologies is the fact that they incur quite large capital expenditures (CAPEX)—especially in continuous processes, as not only the scrubbing units but also regeneration units to recycle the sorption agents are needed. Subsequently, retrofitting existing processes using absorption/adsorption systems tends to be difficult and expensive [9–11]. This is especially problematic for small- and medium-sized companies.

A promising alternative is carbon capture units based on membrane separation. The flue gas is fed into a membrane module where—depending on the choice of membrane—one type of gas molecule (e.g., CO_2) is preferentially transported through the membrane; thus, leading to one depleted stream of gas not passing through the membrane (the retentate stream) and one enriched stream across the membrane (the permeate stream) [11,12]. Implementing membrane capture in existing processes is much more straight-forward and requires significantly less effort regarding equipment—aside from the membrane module, only compressor(s) to achieve the required process pressure for carbon capture are needed [13].

Regarding operational cost of membrane technologies, studies have found competitive per-ton CO_2 costs compared to more established absorption-/adsorption units [14]. Table 1 shows a comparison of representative examples. However, often carbon capture is investigated at high flue gas concentrations or for large-scale plants with very high flow rates (from, for instance, concrete plants or coal powered power plants) [15,16].

Table 1. Examples of simulated CO_2 capture cost using different technologies.

Technology	Feed CO_2 Concentration/%	Flow Rate/kg·h^{-1}	Energy Consumption/kWh·t^{-1}	€·t CO_2 [1]	Ref.
membrane	3.96	4.8×10^6	944–1195	99–117	[15]
absorption [3]	3.96	4.8×10^6	2737	102–160	[15]
amine scrubbing (absorption)	~23	3.5×10^5	---	60–78	[17]
membrane	~23	3.5×10^5	252–272 [2]	32–39	[17]
pressure swing adsorption	20	523	155–318	20–42	[18]

[1] Corrected assuming: 1 $ = 0.8918 € and cumulated inflation of 29.43% since 2020 (ref. [15]), cumulated inflation of ~34% since 2014 (ref. [17]), and of ~5.4% since 2023 (ref. [18]). [2] This energy consumption is given as specific energy penalty compared to the process without carbon capture. [3] Pressurized CO_2 Absorption Integrated with Multi-Shaft Gas Turbine and Heat Recovery Steam Cycle.

Carbon capture at low concentrations poses additional challenges, such as large gas volumes per ton CO_2 captured that have to be processed and reduced separation driving forces due to low CO_2 partial pressures [19,20]. Specifically for membrane capture, these challenges introduce additional requirements like large membrane areas and the above-mentioned feed compression or, alternatively, vacuum generation on the permeate side [14,21,22]. Therefore, simulations of small-scale processes (with low CO_2 concentrations and small flue gas flow rates) often include vacuum pumping and/or using membrane of extremely low thickness (to offset area requirements) [23,24].

To assess the viability of membrane capture as straight-forward retrofit option specifically at low-concentration flue gases, performance data and cost estimates are needed. In this study, the performance of small-scale carbon capture using membrane technology from flue gases with low CO_2 concentrations and small flow rates is modeled without including vacuum pumping, while using membrane thicknesses more fit for industrial use. Performance evaluations for three test cases (CO_2 contents ranging from 1.1% to 5.9%, feed gas flows varying between 1775 kg·h^{-1} and 19,500 kg·h^{-1}) are performed using the process-simulation package Aspen Plus 15.0 [25] and the program MEMSIC 2.0 [26]. Cost estimates per ton CO_2 are obtained by calculating the electricity consumption of the necessary feed compression stages using Aspen HYSYS 15.0 [27]. These estimates serve as a lower bound for capture cost, as equipment investments—those are highly dependent on the specific process—and cost items such as membrane cost are omitted.

2. Materials and Methods

Aspen Plus 15.0 [25] in combination with the MEMSIC 2.0 program [26] (integrated via the CAPE-OPEN standard, to include a membrane separation model) were utilized to simulate the performance of various CO_2 separation membranes with respect to the separation of nitrogen–carbon dioxide mixtures.

Gas streams were treated by employing the IDEAL physical property method as implemented in Aspen Plus. The membrane separation was modeled with a hybrid approach using constant permeabilities and cross plug flow conditions as implemented in MEMSIC (implementation details are described by Bounaceur et al. in [26]).

The membrane module was modeled consisting of three streams (one inlet and two outlet streams) as depicted in the schematic representation in Figure 1: (i) the flue gas (or feed) stream derived from exhaust gases, (ii) the CO_2-poor retentate stream that is the fraction of the feed not passing through the membrane, and (iii) the CO_2-rich permeate stream that is the fraction of the feed that crosses through the membrane.

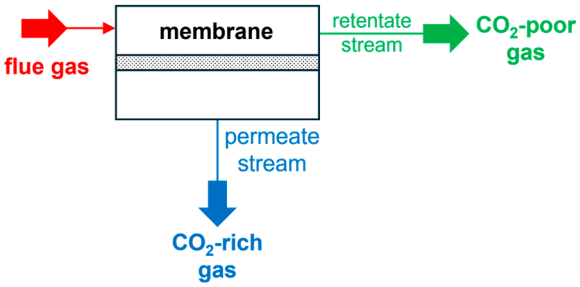


Figure 1. Schematic representation of the simulated membrane module. Three streams are modeled: (i) the flue gas stream (feed stream, red) from the exhaust gases, (ii) the CO_2-poor retentate stream (green) corresponding to the feed fraction remaining upstream, and (iii) the CO_2-enriched permeate stream (blue) corresponding to the feed fraction crossing the membrane.

The separation of the N_2/CO_2 mixtures of varying CO_2 concentration as feed was simulated using 5 different membranes characterized by their permeabilities P_{CO_2} and P_{N_2}, respectively, as well as the selectivity for the gas pair CO_2/N_2 given by:

$$\alpha_{CO_2/N_2}[-] = \frac{P_{CO_2}[\text{barrer}]}{P_{N_2}[\text{barrer}]}\,. \tag{1}$$

$$\text{with1 barrer} = 10^{-10}\frac{\text{cm}^3\cdot\text{cm}}{\text{cm}^2\cdot\text{s}\cdot\text{cmHg}} \tag{2}$$

$$\text{or in SI units : 1 barrer} \approx 3.35\times10^{-16}\frac{\text{mol}\cdot\text{s}}{\text{kg}} \tag{3}$$

In this work, the permeabilities are given in the non-SI unit barrer that relates the gas flow rate (given in $cm^3 \cdot s^{-1}$ using the ideal gas law) to the thickness (in cm) and the area of the membrane (in cm^2) as well as the pressure difference before and after the membrane (in cmHg).

The membrane material parameters are given in Table 2. Note that while the properties of membranes 1–3 were taken from the literature [28–30], the properties of the membranes 4 and 5 were chosen manually: Membrane 4, which was used only to study the influence of the membrane area, was chosen as "low-selectivity membrane". After the single-stage performance tests (see Section 3), Membrane 5 was chosen for the multi-membrane setups with representative values for selectivity and permeabilities (see below).

Table 2. Membrane parameters for the simulated membranes Mem1 to Mem5.

	Mem1	Mem2	Mem3	Mem4 [1]	Mem5 [2]
α_{CO_2/N_2}	14.7	60	30	5	20
P_{CO_2}/barrer	3496	1136	14,000	2000	7000
P_{N_2}/barrer	238	18.93	466.67	400	350
reference	[28]	[29]	[30]	-	-

[1] Only used for area study. [2] Used for multi-membrane setups.

Three main process parameters were taken into account for the single-stage membrane modules: (i) the membrane area A (m^2), (ii) the membrane thickness d (µm), and (iii) the pressure ratio between up- and downstream of the membrane (defined as the quotient of the pressure of the flue gas feed and the pressure of the permeate, respectively).

As mentioned, cross plug flow conditions and constant permeabilities for the studied membranes were assumed for all simulations, and the pressure drop across the membrane was achieved by reducing the downstream pressure in the case of single membranes. For multi-membrane setups, the downstream pressure was set to 1 bar, and the pressure of the feed was increased according to the respective pressure ratio chosen by introducing an additional compression step.

First, the single-stage performance (i.e., of a single membrane) depending on membrane and process parameters was investigated to find suitable values for the thickness and pressure ratios for the multi-membrane setups.

To assess the separation performance, the CO_2 capture rate, the permeate fraction and the CO_2 concentration of the permeate stream were compared. The CO_2 capture rate (CCR, in %) is defined as the fraction of CO_2 in the feed that crosses the membrane and is contained in the permeate stream:

$$\mathrm{CCR}[\%] = \frac{\text{amount of } CO_2 \text{ in permeate stream } [\mathrm{kg \cdot h^{-1}}]}{\text{amount of } CO_2 \text{ in feed stream } [\mathrm{kg \cdot h^{-1}}]}, \quad (4)$$

and the permeate fraction (PF, in %) describes the fraction of the feed stream that permeates the membrane:

$$\mathrm{PF}[\%] = \frac{\text{permeate mass flow } [\mathrm{kg \cdot h^{-1}}]}{\text{feed mass flow } [\mathrm{kg \cdot h^{-1}}]}. \quad (5)$$

Using the results of the single-membrane simulations, parameters were chosen for the multi-membrane setups: Membrane thicknesses were set to the same value within a given multi-membrane setup; however, two different thicknesses were used for different modules ($d = 1$ µm for setups 1 and 3 and $d = 0.5$ µm for setup 2). The pressure ratio was fixed at 5 (meaning all feed streams were compressed to 5 bar and a pressure drop to 1 bar across the membranes was assumed in all simulations). With regard to material properties of the membranes used, $P_{CO_2} = 7000$ barrer and $P_{N_2} = 350$ barrer (leading to $\alpha = 20$) were

chosen. The used membrane area was tailored to the respective flue gas flows and varied case by case.

The CO_2 separation was considered sufficient as soon as the CCR reached values >80%, the PF remained below 20% (in order to achieve a significant reduction in exhaust gas volume) and the residual CO_2 content of the clean exhaust gas (i.e., the retentate stream) was below 1%—please note that configurations that were found to satisfy these constraints are not necessarily the "best" possible ones. Due to MEMSIC being unable to perform automated sensitivity analyses of membrane parameters, all membrane parameter combinations had to be tested manually.

Three different setups were considered (schematics in Figure 2):

1. Two membranes in series, where the retentate stream of the first membrane serves as the feed stream for the second, and the permeate streams are mixed. This setup only uses one initial compression step in which the feed stream is compressed to the initial pressure.
2. Three membranes with a recycling stream (the permeate stream of membrane 3) fed back into the feed stream of membrane 1. The permeate of membrane 1 is used as feed for membrane 2. Subsequently, the retentate streams 1 and 2 are combined into the feed stream of membrane 3. This setup needs two compression steps: the first one processes the combined feed/recycle stream, and the second compresses the permeate stream of membrane 1 to 5 bar before entering membrane 3).
3. A cascade of membrane modules, where the retentate of the previous membrane serves as the feed for the next. In this study, four membranes were used, and the respective membrane areas were chosen such that the criterion of residual CO_2 below 1% in each retentate stream was fulfilled. Notably, this setup needs one compression step per membrane that compresses the permeate stream of the prior membrane to be used as feed stream for the next one.

The sample cases (CO_2 contents and flue gas flows) are summarized in Table 3.

Table 3. Flue gas parameters for different cost estimation cases.

	Case 1	**Case 2**	**Case 3**
CO_2 content/%	1.1	3.0	5.3
flue gas flow/kg·h^{-1}	5680	1775	19,500

The results of the membrane performance investigation with respect to the process parameters are summarized in Section 3.1. The separation performance of the multi-membrane setups is presented in Section 3.2. Additionally, cost estimates C_{CO_2} (in €·t^{-1} CO_2 captured) for sample cases (cf. Table 3) are presented as well, where the electricity cost of the compression steps was taken as proxy. The cost per ton CO_2 captured was calculated according to Equation (6):

$$C_{CO_2}\left[€\cdot t^{-1}_{captured}\right] = \frac{1000}{\dot{P}\left[kg\cdot h^{-1}\right]\cdot x_{CO_2,Permeate}[\%]}\cdot \dot{W}_{comp}[kW]\cdot C_{elec}\ [€\cdot kWh], \quad (6)$$

where $\dot{P}$ denotes the permeate rate, $x_{CO_2,Permeate}$ is the concentration of CO_2 in the permeate feed, $\dot{W}_{comp}$ is the compressor power, and C_{elec} is the electricity cost.

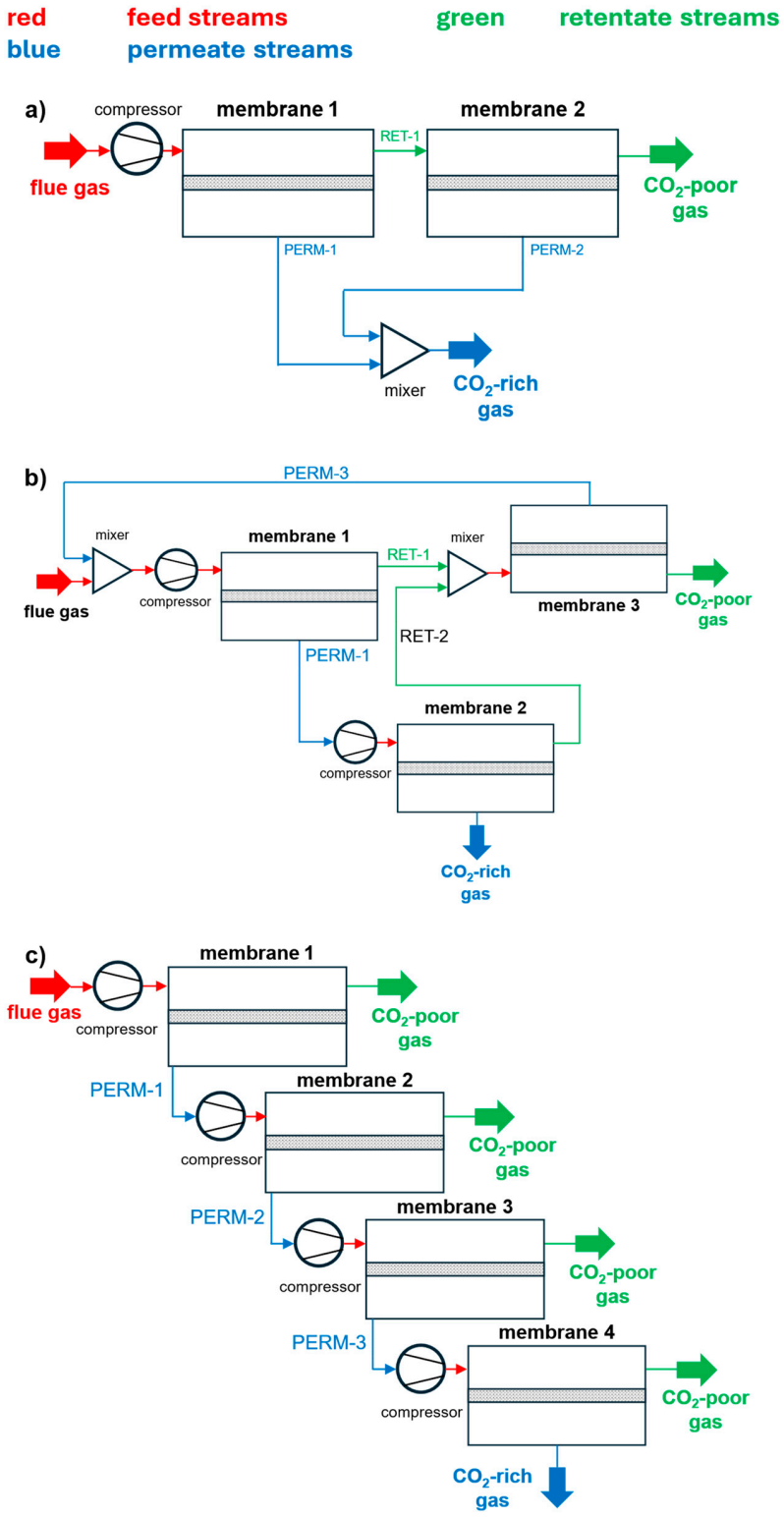


Figure 2. Simulated multiple-membrane setups. (**a**) Two membrane modules in series, where the retentate stream of the first is the feed of the second. (**b**) Three membrane modules with recycle stream (the permeate stream of membrane 3 is fed back and mixed into the feed of membrane 1). The permeate stream of membrane 1 is compressed and used as feed for membrane 2, with retentate streams of membranes 1 and 2 combined and fed into membrane 3. (**c**) A cascade of membrane modules (in the case of this work, four modules have been used). The retentate stream of the previous membrane is compressed and used as feed stream for the next stage. In all flow charts, feed streams are shown in red, retentate streams in green, and permeate streams in blue.

The compressor power needed for these estimates was calculated with Aspen HYSYS 15.0 [27] employing a single-stage adiabatic compression model (an adiabatic efficiency of 75% was assumed) and a Peng-Robinson fluid package as implemented in Aspen HYSYS. The inlet flows and the molecular weight of the respective gas streams (either feed streams or permeate streams) were taken from Aspen Plus/MEMSIC calculations. The inlet temperature was set to 25 °C and the outlet pressure was set to 5 bar (given by the feed stream requirements of the multi-membrane setups).

3. Results

3.1. Performance of Single Membranes

In the following section, the detailed results of the single-membrane performance are summarized.

3.1.1. Impact of Pressure Ratio

The impact of the pressure ratio between up- and downstream pressure was modeled for the membranes 1–3 (cf. Table 1) using a constant area of 1000 m^2 and a thickness of 1 µm. To assess different trends, the flue gas flow was varied between 500 kg·h^{-1} and 20,000 kg·h^{-1}, and the CO_2 concentration was varied between 1% and 15% (with N_2 making up the rest of the mixture). Figure 3 illustrates the typical behavior: The CO_2 concentration in the permeate stream (plotted on the secondary axes) increases to some maximum, beyond which it drops again for higher pressures—at this point, all present CO_2 has passed through the membrane and further pressure increases only force more N_2 through the membrane into the permeate stream, thus decreasing the concentration of CO_2 again. Increasing the flow rate shifts this maximum to the right (the maximum concentration on the left—flow rate: 2000 kg·h^{-1}— of about 11.5% CO_2 occurs with a pressure ratio of roughly 10, on the right—flow rate: 3000 kg·h^{-1}—the maximum has not been definitely reached, as the CCR was still just below 100%). Both CCR and CO_2 concentration increase fairly linearly up to a pressure ratio of 4 to 5. Beyond that, the slope begins to level off.

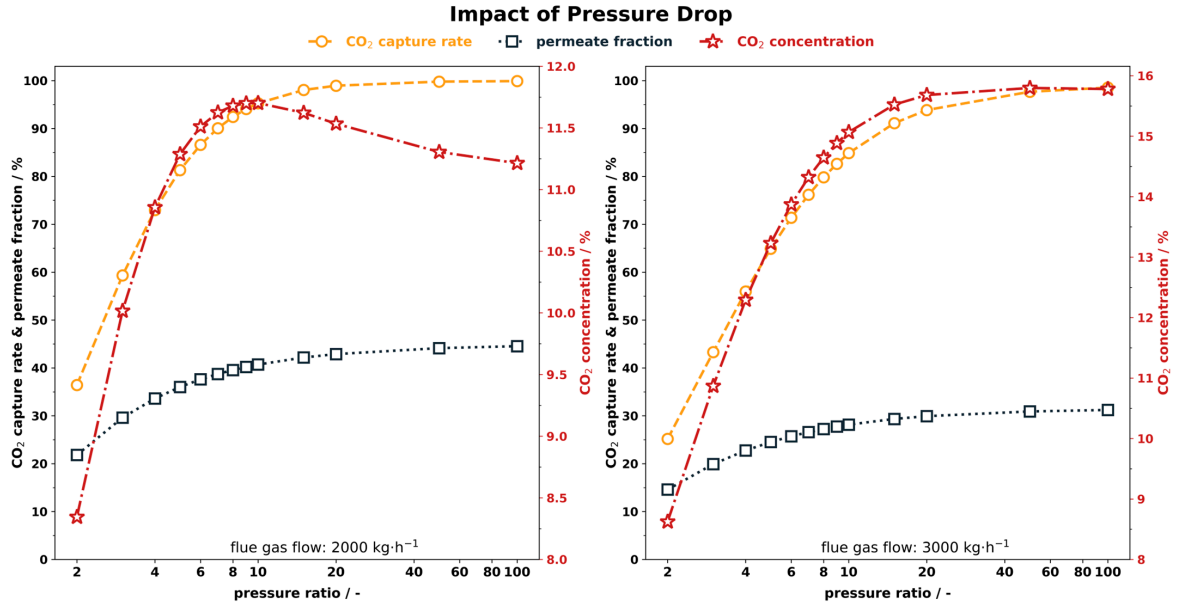


Figure 3. Impact of pressure drop between feed and permeate streams. Shown are the results for Mem1 (A = 1000 m^2, d = 1 µm) with flow rates of 2000 kg·h^{-1} (**left**) and 3000 kg·h^{-1} (**right**) and a CO_2 concentration of 7% in the flue gas.

The exact qualitative shape of the curves depends on all possible membrane parameters, e.g., too low permeabilities might lead to a significantly smaller slope of the concentration curve. However, this can be offset by an adjustment of the area and thickness of the membrane; therefore, a pressure ratio of 5 (which was chosen for the multi-membrane setups) appears to be a good tradeoff between compression requirements and increased efficiency—especially with respect to the expected electricity cost of compression.

3.1.2. Influence of Membrane Thickness

The influence of the membrane thickness was modeled for the membranes 1–3 (cf. Table 1) using a constant area of 1000 m^2 and a pressure ratio of 4. To assess different trends, the flue gas flow was varied between 500 $kg \cdot h^{-1}$ and 20,000 $kg \cdot h^{-1}$, and the CO_2 concentration of the feed stream was varied between 1% and 15% (with N_2 making up the rest of the mixture). Figure 4 illustrates the typical behavior with two representative plots.

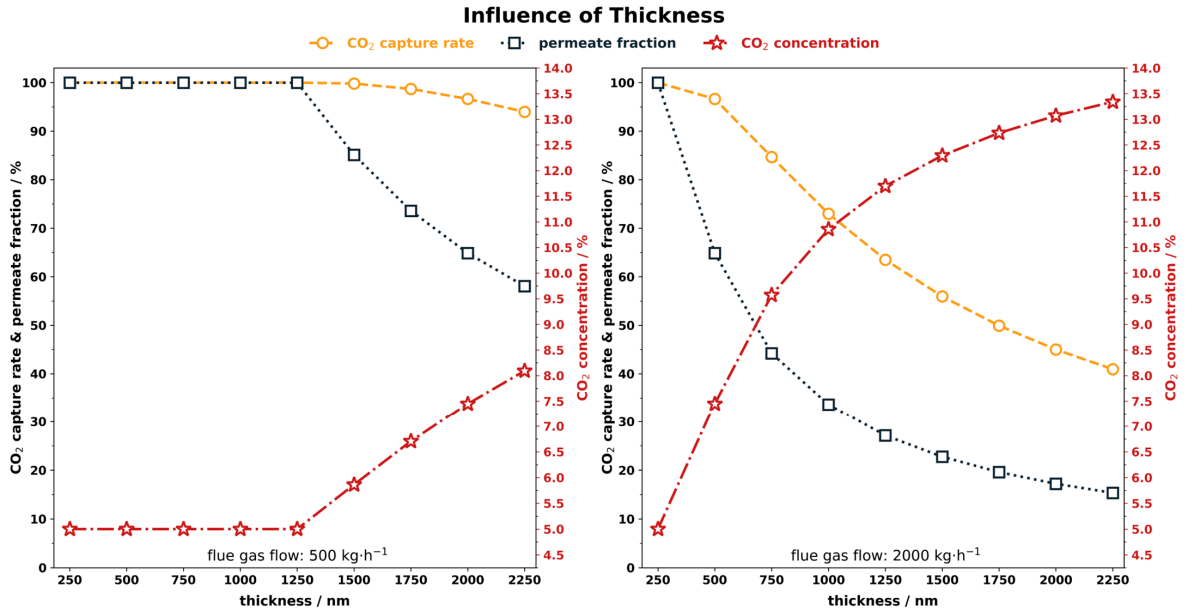


Figure 4. Influence of membrane thickness. Shown are the results for Mem1 (A = 1000 m^2, pressure ratio 4) with a flow rate of 500 $kg \cdot h^{-1}$ (**left**) and 2000 $kg \cdot h^{-1}$ (**right**). In both cases, the CO_2 concentration of the flue gas was 5%.

Unsurprisingly, both CCR and PF decrease with increasing thickness. The main difference between the simulated membrane units is whether separation occurs and at what minimum thickness it starts: In cases where the permeability of the membrane was too high for a given (low) flow rate (for instance Mem1 and 500 $kg \cdot h^{-1}$; Figure 4 left) and a small thickness, the entire feed stream could pass through the membrane. In such cases, a thicker membrane has to be chosen (or alternatively, the area of the membrane module has to be reduced) in order to facilitate separation.

For the simulations, where separation is achieved, two possible cases were observed: (i) both CCR and PF reached 100% (or close to) for smaller thicknesses or (ii) the CCR did not reach (close to) 100%. In the former case, there is a range of thicknesses where the CCR decreases more slowly with increasing thickness than the PF (in the right diagram of Figure 4 between 250 nm and roughly 1000 nm). This means that there is an optimal thickness with respect to separation efficiency. In the second case, CCR drops faster with thickness than PF over the whole range considered, meaning that the smallest investigated thickness (250 nm) is the optimal one. It is to be expected that going to even thinner membranes, an optimum for the thickness would appear in the second case as well.

The concentration of the permeate stream (plotted on the secondary axes of Figure 4) only starts to increase when no longer 100% of the feed stream permeates through the membrane.

Changes in the feed stream concentration do not change the qualitative shape of the CCR and PF curves—increasing feed concentration increases the minimum thickness necessary to achieve separation for a given flue gas flow, and affects the maximum permeate concentration achievable in the investigated thickness range.

A thickness of 1000 nm was chosen for the 2- and 4-membrane setups, 500 nm thick membranes were used in the 3-membrane simulations.

3.1.3. Effect of Membrane Area

The effect of the membrane area was modeled for the membranes 1–4 (cf. Table 1) using a constant thickness of 1 µm and a pressure ratio of 4. To assess different trends, the flue gas flow was varied between 500 kg·h^{-1} and 20,000 kg·h^{-1} and the CO_2 concentration was varied between 1% and 15% (with N_2 making up the rest of the mixture). Figure 5 illustrates the typical behavior.

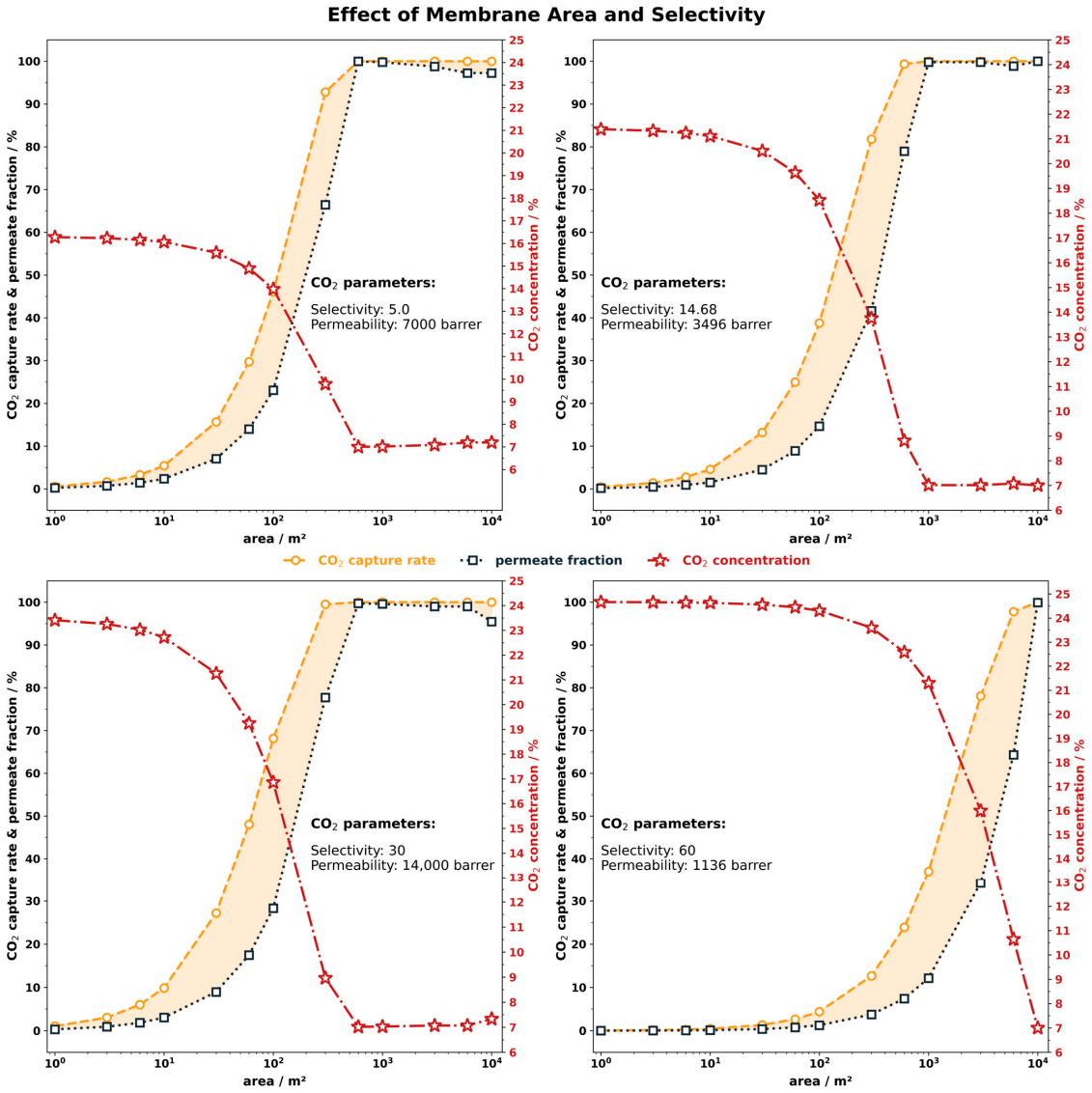


Figure 5. Effect of membrane area. Shown are the results for membranes 1–4 with varying selectivities and permeabilities and d = 1 µm, pressure ratio 4, a flow rate of 500 kg·h^{-1}, and a CO_2 concentration of 7% in the flue gas. The shaded areas represent the regions where CCR grows faster than PF.

The basic shape of the curves is the same for all membranes, independently of permeability and selectivity: For small areas, CCR and PF are small (i.e., only a small amount of gas crosses the membrane) while the CO_2 concentration is at the maximum value. With increasing area, CCR grows faster than PF leading to the "loop"-like shape highlighted in yellow in Figure 5. Both quantities approach 100% with increasing area (for too large membranes, 100% are reached)—as soon as the permeate fraction reaches 100% as well, the CO_2 content of the permeate stream equals that of the feed stream. The onset of the loop as well as the maximum width depend on the membrane parameters. The permeability affects the onset, with larger permeabilities moving it to smaller areas, while smaller selectivities lead to narrower loops. The differences between the maximum width are less pronounced; however, the smallest selectivity shown in Figure 5 clearly has the smallest maximum width as well. Additionally, selectivity affects the maximum concentration achievable (larger selectivities lead to higher concentrations).

While the initial concentration of the feed has only little effect on the optimal area (it slightly shifts both CCR and PF upward), the flue gas flow rate has a significant impact: Higher flows shift the loop to the right leading to larger optimal areas.

A tradeoff between carbon capture rate and permeate fraction is necessary to facilitate separation. The position of the optimum depends on the permeate requirements (e.g., amount of CO_2 captured, concentration in the permeate …).

3.2. Performance of Multi-Membrane Setups and Cost Estimate

The results of the performance simulations of the three different multiple-membrane modules (cf. Figure 2) are summarized in Tables 3–5. Mem5 (cf. Table 1) was used as membrane type, the pressure ratio was fixed to 5 in all cases, and the membrane thicknesses were set to 1 µm for the 2- and 4-membrane units, while 500 nm thick membranes were used in the model for the 3-membrane unit. Again, please note that a limited number of test cases were performed manually, as automated sensitivity analyses of membrane parameters were not possible with MEMSIC. The presented "best tested setup", therefore, is not necessarily the optimal possible one for the given set of parameters, but the configuration that (i) fulfilled the criteria outlined in Section 2 (CCR > 80% and PF < 20%) and (ii) exhibited the largest CCR of all considered configurations for a given test case (if more than one was found fulfilling these criteria).

Table 4. Performance of best tested setup and cost estimate for the 2-membrane setup.

	Case 1	**Case 2**	**Case 3**
CO_2 content, feed/%	1.1	3.0	5.3
flue gas flow/kg·h^{-1}	5680	1775	19,500
total membrane area/m^2	2000	800	9000
CCR/%	82	91	93
PF/%	35	45	48
CO_2 content, permeate/%	2.6	6.1	10.2
permeate flow rate/kg·h^{-1}	1993	803	9435
CO_2 content, retentate/%	0.3	0.5	0.7
electricity consumption/kWh·t^{-1} CO_2 captured	11,985	3942	2172
estimated cost/€·t^{-1} CO_2	599	197	109

To calculate the estimated cost per ton CO_2 captured based on the electricity consumption of the compression steps, Equation (6) has been used, where a cost of 0.05 €·kWh^{-1} was assumed. This price, while low, was used with the Austrian "Industriestrompreis" (scheduled for 2027) in mind.

Table 5. Performance of best tested setup and cost estimate for the 3-membrane setup.

	Case 1	Case 2	Case 3
CO_2 content, feed/%	1.1	3.0	5.3
flue gas flow/kg·h^{-1}	5680	1775	19,500
total membrane area/m^2	1375	875	7500
CCR/%	82	89	88
PF/%	6	19	19
CO_2 content, permeate/%	11.5	14.4	24.5
permeate flow rate/kg·h^{-1}	319	330	3715
CO_2 content, retentate/%	0.5	0.4	0.8
electricity consumption/kWh·t^{-1} CO_2 captured	17,019	6743	3745
estimated cost/€·t^{-1} CO_2	851	337	187

The results for the dual-membrane units (Table 4) show that the requirements of CCR > 80% and PF < 20% cannot be achieved simultaneously. Therefore, the PF criterion was relaxed. In all three cases, the CO_2 downstream of the membrane could be roughly doubled. The cost per ton CO_2 decreases almost linearly with the flue gas concentration.

The 3-membrane module with a recycling stream yields significantly better results (Table 5) than the dual-membrane unit with comparable or even smaller total membrane areas. However, due to the different thicknesses used in the three-membrane setup, it is unclear if the improved performance originates from the different parameters or the changed flow chart. The CO_2 concentration of the flue gas could be increased by a factor of 4–6 in the permeate stream. Due to the additional compression step, electricity cost is higher.

Using four membranes allows for even higher concentrations in the permeate stream (Table 6), albeit with much larger membrane areas and higher electricity cost (due to four compression stages in total). This setup is quite flexible, as the membranes can be tuned independently in accordance with the requirements for permeate and retentate streams, respectively, and additional membranes can easily be added if necessary.

Table 6. Performance of best tested setup and cost estimate for the 4-membrane setup.

	Case 1	Case 2	Case 3
CO_2 content, feed/%	1.1	3.0	5.3
flue gas flow/kg·h^{-1}	5680	1775	19,500
total membrane area/m^2	5650	2315	18,500
CCR/%	82	93	87
PF/%	8	16	14
CO_2 content, permeate/%	12.0	17.4	32.7
permeate flow rate/kg·h^{-1}	428	322	2768
CO_2 content, retentate/%	0.1–0.6	0.3–0.7	0.6–0.8
electricity consumption/kWh·t^{-1} CO_2 captured	22,937	7532	4369
estimated cost/€·t^{-1} CO_2	1147	377	219

4. Discussion

Before discussing the results in more detail, the two fundamental assumptions made for all the above-shown simulations need to be justified. These are (i) constant permeability (i.e., the material properties of the simulated membranes do not degrade, and there is no gradient through the membrane) and (ii) cross plug flow conditions (i.e., steady flow along the membrane without concentration gradients near the it). Both assumptions were applied for simplification: The Performance depends strongly on process specifics (such

as flue gas temperature and pressure, possible contaminants, geometry of the membrane module, state and stability of the membrane, and so on). To generate estimates that do not hinge on process specifics, conditions such as steady states (stable temperature, pressure, feed composition, no contaminants) and clean, uniform membranes were assumed. In the case of downstream retrofitted membrane modules, such conditions can be achieved by including process-specific flue-gas treatment (like temperature control or contaminant removal) [31–34].

The single-membrane simulations (Figures 3–5) clearly demonstrate the interdependency of membrane area, thickness, and pressure ratio, meaning the membrane separation can be tuned very efficiently by varying one/several of these parameters depending on the specifics of the process (available membrane type, flue gas flow rate, CO_2 content ...):

In Figure 3, the characteristic response of carbon capture rate (CCR) and permeate fraction (FR) to increasing pressure ratio is shown: Initially, the achieved CCR grows faster with the pressure ratio than PF due to higher CO_2 permeability (P_{CO_2}), consequently leading to larger CO_2 concentration in the permeate feeds—with concentrations responding linearly to the increased pressure ratio. The CCR approaches 100% with decreasing growth rates, while PF continues to increase (possibly faster than CCR). This subsequently leads to a leveling-off (or even decrease) of the CO_2 concentration. Whether a maximum concentration is observed in a given pressure ratio range or the concentration simply approaches a maximum depends on the process specifics (feed concentration and flow rate). As the pressure difference across the membranes in this study was achieved exclusively via feed stream compression, there is a tradeoff between separation efficiency and electricity cost of compression.

Figure 4 illustrates changes in CCR, PF, and CO_2 concentration with increasing membrane thickness: For thicker membranes, the transport through the membrane is more difficult, which leads to smaller values CCR and PF. Conversely, the CO_2 concentration increases for larger thicknesses. The observed shape of the curves can be explained quite straight-forwardly: For thin membranes (and small feed flows relative to the membrane area), the entire feed stream can permeate (CCR = PF = 100%), and the CO_2 concentration in the permeate stream equals that in the feed stream. At some critical thickness, the feed can no longer permeate in its entirety and CCR and PF diverge, because the CCR decreases more slowly than PF (again because of $P_{CO_2} > P_{N_2}$), subsequently causing an increase in the CO_2 concentration in the permeate. The growth of the concentration slows down as the membrane thickness increases further and both CCR and PF start to decrease more slowly, approaching its maximum value in the limit of CCR = PF = 0%). This means there is another tradeoff at play: Thin membranes lead to high values for CCR but do not lead to sufficient permeate concentrations (as PF is also high), while thick membranes cause CO_2 enrichment in the permeate stream but decrease CCR.

Figure 5 shows the responses of CCR, PF, and CO_2 permeate concentration to changes in the membrane area for different membrane parameters: The fundamental shape of the curves is the same for all membranes (independent of permeability and selectivity). For small areas, CCR and PF are small as only a small fraction of the feed stream permeates through the membrane, while the permeate CO_2 content is at a maximum value. With increasing area, CCR grows faster than PF leading to a feature reminiscent of a hysteresis loop. If the area grows even larger, both CCR and PF approach 100%, at which point the permeate CO_2 concentration has dropped to the initial CO_2 concentration in the feed stream, as the entire feed can permeate through the membrane. This means that meaningful separation is possible only within this loop. The onset area (where the loop begins to open) and the maximum width of the loop depend on the membrane parameters: The permeabilities influence the onset of the loop—larger permeabilities move it to smaller

areas, while selectivity affects the width—a larger selectivity leads to a wider loop. The process parameters play a role as well. While the feed concentrations have only a small effect on the optimal area (higher feed content slightly shifts CCR and PF upward), the flue gas rate has a larger influence—higher flows shift the loop to the right.

All single-membrane simulations quite clearly show that the criteria for "successful" separation (CCR > 80%, PF < 20%) used in this study, cannot be achieved with a single membrane alone, and a series of three or more membranes are needed to achieve satisfactory carbon capture rates and CO_2 reduction in the retentate stream (i.e., cleaned flue gas).

The performance simulations of multi-membrane modules show two general trends across all setups:

First, both the capture cost and the electricity consumption per ton of CO_2 captured decrease with increasing CO_2 concentration in the feed. This behavior is expected for membrane systems, since low-concentration feeds require compression and handling of relatively large amounts of non-permeating gas per ton of CO_2 [21,22].

Second, the total membrane area required to achieve sufficient separation grows with the feed flow rate.

In terms of CCR, PF, and CO_2 content in the permeate, the simulations show that 2-membrane modules do not enable sufficient separation; notably, the PF < 20% requirement could not be achieved simultaneously with a CCR > 80% (cf. Table 4). Accordingly, only a moderate CO_2 enrichment—approximately by a factor of 2 relative to the feed stream—was obtained in the permeate stream.

For 3- and 4-membrane setups (Tables 5 and 6, respectively) both requirements could be fulfilled. Consequently, the CO_2 concentration in the permeate could be increased to approximately 480% to more than 1000% of the respective feed concentration. A direct comparison between the 3- and 4-membrane configurations, however, does not reveal sufficiently large differences to conclusively identify one configuration as superior in the tested cases. Again, this result confirms expectations, as multi-stage membrane configurations are widely seen as potential means to improve the separation from dilute feed streams, although additional stages usually increase membrane area, compression duty, and capital cost [21,22,35].

It should be noted that the results presented correspond to the best tested membrane-area combination for each feed case and module configuration. In this context, "best tested" does not imply that the process design was fully optimized, because the tested configurations were chosen and varied manually. Further optimization—ideally as part of an automated sensitivity analysis—is needed to discern which of those setups yields better results.

Regarding the capture cost per ton of CO_2, the feed streams with the lowest concentration incurred the highest compression cost (going from 599 €·t^{-1} for the 2-membrane to 1147 €·t^{-1} for the 4-membrane setup). For the medium-concentration case the capture cost falls in the range of 197–377 €·t^{-1}, and the highest considered concentration leads to cost estimates between 109 and 219 €·t^{-1}.

Unsurprisingly, the cost-per-ton reported in the literature for flue gases with high CO_2 concentrations (>10%) were significantly exceeded:

For example, Lindqvist et al. report an expected cost of around 35 €·t^{-1} CO_2 (converted assuming a cumulated inflation of ~34% since 2014) in a techno-economic analysis of retrofitting a concrete plant with membrane capture technology [17]. In the same study, absorption-based capture (amine scrubbing) with an associated per-ton cost of 68 €·t^{-1} CO_2 (converted assuming a cumulated inflation of ~34% since 2014) and CAPEX estimates more than 4–5 times higher than the membrane process (>200 M€ and 35–50 M€, respectively) was presented as comparison—meaning that for this use case membrane capture is a competitive alternative to absorption-based technologies [17]. Ramasubramanian et al. found a similar

per-ton CO_2 cost (~34 €·t^{-1} CO_2 (converted assuming a cumulated inflation of ~36% since 2012)) in an analysis of membrane capture in a coal power plant [36], and Giordano et al. report 24–40 €·t^{-1} CO_2 (converted from $ assuming an exchange rate of 1 $ = 0.8918 € and cumulated inflation of ~31% since 2017) in a parameter study of membrane systems in similar post-combustion capture applications [23]. The CO_2 concentrations were ~23% in the former and ~13% in the two latter examples, while the feed flows were multiple orders of magnitude (>10^5 kg·h) larger than the cases investigated in this study [17,23,36]. This trend of decreasing cost with higher concentrations could be observed in this study as well: Increasing the CO_2 content from 1% to 5% significantly reduces the cost estimates—the 2-membrane configuration (cf. Table 4) exhibits an almost linear cost reduction.

Previous studies with membrane capture at low concentrations (<10%) estimate significantly smaller per-ton cost as well: Gatti et al. find 99–117 €·t^{-1} CO_2 (converted from $ assuming an exchange rate of 1 $ = 0.8918 € and cumulated inflation of ~30% since 2020) at ~4% CO_2 content in an analysis of a natural gas-fired power plant [15], and Adhikari et al. find around 49 €·t^{-1} CO_2 (converted from $ assuming an exchange rate of 1 $ = 0.8918 € and cumulated inflation of ~5.4% since 2023) at 1% CO_2 in a recent techno-economic analysis [24].

However, many of those results model the process with additional vacuum pumping [15,17,23], very thin membranes [23,24], and/or do not take compression of the membrane capture costs into account [24]. These choices were intentionally not replicated in the models of this work, as the main goal was the assessment of the feasibility of a "straight-forward" retrofitting of small-to-mid-sized plants by simply adding membrane separation downstream of an existing process.

5. Conclusions

(1) The process parameters of area, thickness, and pressure ratio are interdependent with respect to their impact on capture performance, meaning the membrane separation can be tuned very efficiently varying one or all parameters depending on the specifics of the process (available membrane type, flue gas flow rate, CO_2 content ...).
(2) A single membrane is not sufficient to achieve the target parameters CCR > 80% and PF < 20% simultaneously, and a series of three or more membranes are needed to achieve satisfactory carbon capture rates and CO_2 reduction in the retentate stream (i.e., cleaned flue gas).
(3) The cost per-ton CO_2 reported in the literature (e.g., [17,23,36]) for flue gases with higher (>10%) CO_2 concentrations was significantly exceeded.
(4) Capture costs reported in the literature (e.g., [15,24]) at lower CO_2 concentrations (<10%) were exceeded as well.
(5) However, many results reported use vacuum pumping or very thin membranes; and/or do not take compression costs into account. These choices were intentionally not replicated in the models of this work, as the main goal was the assessment of the feasibility of a "straight-forward" retrofitting of small-to-mid-sized plants by simply adding membrane separation downstream of an existing process.
(6) The results of this work clearly highlight the necessity of more sophisticated engineering approaches (versus simple addition of downstream membranes) to achieve efficient, affordable CO_2 capture at low CO_2 concentrations.

Author Contributions: Conceptualization, T.R. and C.R.; methodology, T.R.; validation, T.R. and C.R.; formal analysis, T.R.; investigation, T.R.; data curation, T.R.; writing—original draft preparation, T.R.; writing—review and editing, T.R. and C.R.; visualization, T.R.; supervision, C.R.; project administration, C.R.; funding acquisition, C.R. All authors have read and agreed to the published version of the manuscript.

Funding: This research was funded by the Agency for Education and Internationalization (OeAD) on behalf of the Austrian Ministry of Women, Science and Research under the Sparkling Science 2.0 program (project SPSC_01_015–CO2 Umwandlung). The APC was funded by the University Library of the Montanuniversität Leoben.

Data Availability Statement: The raw data supporting the conclusions of this article will be made available by the authors on request.

Conflicts of Interest: The authors declare no conflicts of interest.

Abbreviations

The following abbreviations are used in this manuscript:

CAPEX	Capital Expenditures
CCR	CO_2 Capture Rate [%], cf. Equation (4)
CCU	Carbon Capture and Utilization
OPEX	Operational Expenditures
PF	Permeate Fraction [%], cf. Equation (5)

References

1. Intergovernmental Panel on Climate Change (IPCC). *Climate Change 2013: The Physical Science Basis. Contribution of Working Group I to the Fifth Assessment Report of the Intergovernmental Panel on Climate Change*; Cambridge University Press: Cambridge, UK; New York, NY, USA, 2013.
2. Intergovernmental Panel on Climate Change (IPCC). *Climate Change 2022: Impacts, Adaptation and Vulnerability. Contribution of Working Group II to the Sixth Assessment Report of the Intergovernmental Panel on Climate Change*; Cambridge University Press: Cambridge, UK; New York, NY, USA, 2022.
3. European Commission. The European Green Deal. Available online: https://commission.europa.eu/strategy-and-policy/priorities-2019-2024/european-green-deal_en (accessed on 7 September 2026).
4. Simon Araya, S.; Liso, V.; Cui, X.; Li, N.; Zhu, J.; Sahlin, S.L.; Jensen, S.H.; Nielsen, M.P.; Kær, S.K. A Review of The Methanol Economy: The Fuel Cell Route. *Energies* **2020**, *13*, 596. [CrossRef]
5. Centi, G.; Perathoner, S. Chemistry and energy beyond fossil fuels. A perspective view on the role of syngas from waste sources. *Catal. Today* **2020**, *342*, 4–12. [CrossRef]
6. Falkowski, P.; Scholes, R.J.; Boyle, E.; Canadell, J.; Canfield, D.; Elser, J.; Gruber, N.; Hibbard, K.; Hogberg, P.; Linder, S.; et al. The global carbon cycle: A test of our knowledge of earth as a system. *Science* **2000**, *290*, 291–296. [CrossRef] [PubMed]
7. Luhar, S.; Ashour, A.; Luhar, I. Decarbonising the Cement and Concrete Industry—A Step Forward to a Sustainable Future. *J. Compos. Sci.* **2026**, *10*, 226. [CrossRef]
8. Liang, L.Z.; Macdonald, J.H.; Kamaruzaman, N.; Thangalazhy-Gopakumar, S.; Azmi, A.A.; Abbas, A.; Shah, N.; Abdul Manaf, N. Operational insights into a biomass gasification with carbon capture as a CO_2 removal technology. *Energy* **2026**, *351*, 140756. [CrossRef]
9. Bains, P.; Psarras, P.; Wilcox, J. CO_2 capture from the industry sector. *Prog. Energy Combust. Sci.* **2017**, *63*, 146–172. [CrossRef]
10. Vaz, S.; Rodrigues de Souza, A.P.; Lobo Baeta, B.E. Technologies for carbon dioxide capture: A review applied to energy sectors. *Clean. Eng. Technol.* **2022**, *8*, 100456. [CrossRef]
11. Hekmatmehr, H.; Esmaeili, A.; Pourmahdi, M.; Atashrouz, S.; Abedi, A.; Ali Abuswer, M.; Nedeljkovic, D.; Latifi, M.; Farag, S.; Mohaddespour, A. Carbon capture technologies: A review on technology readiness level. *Fuel* **2024**, *363*, 130898. [CrossRef]
12. Hou, R.; Fong, C.; Freeman, B.D.; Hill, M.R.; Xie, Z. Current status and advances in membrane technology for carbon capture. *Sep. Purif. Technol.* **2022**, *300*, 121863. [CrossRef]
13. Obi, D.; Onyekuru, S.; Orga, A. Review of recent process developments in the field of carbon dioxide (CO_2) capture from power plants flue gases and the future perspectives. *Int. J. Sustain. Energy* **2024**, *43*, 2317137. [CrossRef]
14. Merkel, T.; Baker, R.; Hao, P.; Kniep, J.; He, Z.; Huang, Y.; Salim, W. Carbon capture with membranes: An opportunity revisited. *J. Membr. Sci.* **2026**, *738*, 124829. [CrossRef]
15. Gatti, M.; Martelli, E.; Di Bona, D.; Gabba, M.; Scaccabarozzi, R.; Spinelli, M.; Viganò, F.; Consonni, S. Preliminary Performance and Cost Evaluation of Four Alternative Technologies for Post-Combustion CO_2 Capture in Natural Gas-Fired Power Plants. *Energies* **2020**, *13*, 543. [CrossRef]
16. Micari, M.; Hsu, K.-J.; Bempeli, S.; Agrawal, K.V. Energy- and cost-efficient CO_2 capture from dilute emissions by pyridinic-graphene membranes. *Nat. Sustain.* **2025**, *9*, 164–175. [CrossRef]

17. Lindqvist, K.; Roussanaly, S.; Anantharaman, R. Multi-stage Membrane Processes for CO_2 Capture from Cement Industry. *Energy Procedia* **2014**, *63*, 6476–6483. [CrossRef]
18. Tingelinhas, J.; Saragoça, C.; Al Mohtar, A.; Mateus, M.; Pinto, M.L. Pillared Clays as Cost-Effective Adsorbents for Carbon Capture by Pressure Swing Adsorption Processes in the Cement Industry. *Ind. Eng. Chem. Res.* **2023**, *62*, 5613–5623. [CrossRef]
19. Rao, A.B.; Rubin, E.S. Identifying Cost-Effective CO_2 Control Levels for Amine-Based CO_2 Capture Systems. *Ind. Eng. Chem. Res.* **2005**, *45*, 2421–2429. [CrossRef]
20. House, K.Z.; Harvey, C.F.; Aziz, M.J.; Schrag, D.P. The energy penalty of post-combustion CO_2 capture & storage and its implications for retrofitting the U.S. installed base. *Energy Environ. Sci.* **2009**, *2*, 193–205. [CrossRef]
21. Favre, E. Carbon dioxide recovery from post-combustion processes: Can gas permeation membranes compete with absorption? *J. Membr. Sci.* **2007**, *294*, 50–59. [CrossRef]
22. Merkel, T.C.; Lin, H.; Wei, X.; Baker, R. Power plant post-combustion carbon dioxide capture: An opportunity for membranes. *J. Membr. Sci.* **2010**, *359*, 126–139. [CrossRef]
23. Giordano, L.; Roizard, D.; Bounaceur, R.; Favre, E. Evaluating the effects of CO_2 capture benchmarks on efficiency and costs of membrane systems for post-combustion capture: A parametric simulation study. *Int. J. Greenh. Gas Control* **2017**, *63*, 449–461. [CrossRef]
24. Adhikari, B.; Orme, C.J.; Stetson, C.; Klaehn, J.R. Techno-economic analysis of carbon dioxide capture from low concentration sources using membranes. *Chem. Eng. J.* **2023**, *474*, 145876. [CrossRef]
25. *Aspen Plus*, version 15.0, Aspen Technology, Inc.: Bedford, MA, USA, 2025.
26. Bounaceur, R.; Berger, E.; Pfister, M.; Ramirez Santos, A.A.; Favre, E. Rigorous variable permeability modelling and process simulation for the design of polymeric membrane gas separation units: MEMSIC simulation tool. *J. Membr. Sci.* **2017**, *523*, 77–91. [CrossRef]
27. *Aspen HYSYS*, version 15.0, Aspen Technology, Inc.: Bedford, MA, USA, 2025.
28. Staiger, C.L.; Pas, S.J.; Hill, A.J.; Cornelius, C.J. Gas Separation, Free Volume Distribution, and Physical Aging of a Highly Microporous Spirobisindane Polymer. *Chem. Mater.* **2008**, *20*, 2606–2608. [CrossRef]
29. Gkotsis, P.; Peleka, E.; Zouboulis, A. Membrane-Based Technologies for Post-Combustion CO_2 Capture from Flue Gases: Recent Progress in Commonly Employed Membrane Materials. *Membranes* **2023**, *13*, 898. [CrossRef] [PubMed]
30. Pu, Y.; Yang, Z.; Wee, V.; Wu, Z.; Jiang, Z.; Zhao, D. Amino-functionalized NUS-8 nanosheets as fillers in PIM-1 mixed matrix membranes for CO_2 separations. *J. Membr. Sci.* **2022**, *641*, 119912. [CrossRef]
31. Mulder, M. *Basic Principles of Membrane Technology*, 2nd ed.; Springer: Dordrecht, The Netherlands, 1996.
32. Bacchin, P.; Aimar, P.; Field, R. Critical and sustainable fluxes: Theory, experiments and applications. *J. Membr. Sci.* **2006**, *281*, 42–69. [CrossRef]
33. Baker, R.W. *Membrane Technology and Applications*, 3rd ed.; John Wiley & Sons: Hoboken, NJ, USA, 2012.
34. Schwinge, J.; Neal, P.R.; Wiley, D.E.; Fletcher, D.F.; Fane, A.G. Spiral wound modules and spacers: Review and analysis. *J. Membr. Sci.* **2004**, *242*, 129–153. [CrossRef]
35. Baker, R.W.; Lokhandwala, K. Natural gas processing with membranes: An overview. *Ind. Eng. Chem. Res.* **2008**, *47*, 2109–2121. [CrossRef]
36. Ramasubramanian, K.; Verweij, H.; Winston Ho, W.S. Membrane processes for carbon capture from coal-fired power plant flue gas: A modeling and cost study. *J. Membr. Sci.* **2012**, *421–422*, 299–310. [CrossRef]

Disclaimer/Publisher's Note: The statements, opinions and data contained in all publications are solely those of the individual author(s) and contributor(s) and not of MDPI and/or the editor(s). MDPI and/or the editor(s) disclaim responsibility for any injury to people or property resulting from any ideas, methods, instructions or products referred to in the content.